INSTITUTE OF PHYSICS PUBLISHING METROLOGIA
Metrologia **40** (2003) 1–5 PII: S0026-1394(03)56889-X

Linearity of InGaAs photodiodes

H W Yoon, J J Butler, T C Larason and G P Eppeldauer

Optical Technology Division, NIST, Gaithersburg, MD 20899-8441, USA

Published
Online at stacks.iop.org/Met/40

Abstract
In radiometry or pyrometry, radiometers are often used to assign the spectral radiance or radiance temperatures of sources using ratios of signals which can differ by several decades. For performing ratios between such sources with low uncertainties, the linearity of the detectors used in the transfer radiometers needs to be characterized. The linearity of InGaAs photodiodes has been studied using the flux-addition method using a broadband infrared source with a visible-blocking filter. Using this technique, 18 InGaAs photodiodes from four different vendors were studied without spectral filtering in a broad wavelength region from 900 to 1700 nm with the diodes underfilled by the incident flux. The linearity of InGaAs photodiodes was determined within the range of photocurrents from 10^{-8} to 10^{-4} A. All the InGaAs photodiodes demonstrated linearity from 10^{-7} to 10^{-4} A within the expanded uncertainties of 0.08% ($k = 2$). The uncertainty in the linearity measurement below 10^{-8} A is increased due to the increased noise in the photocurrent arising from the feedback resistance of the transimpedance amplifier being greater than the shunt resistance of the photodiode.

1. Introduction

InGaAs photodiodes are critical components in optical networks, and as the manufacturing process for InGaAs improves, they are being increasingly used as detectors in thermal imaging, pyrometry [1] and spectroradiometry [2]. Previously, the electronic characteristics of InGaAs and Ge photodiodes using current preamplifiers were compared, and the InGaAs photodiodes were found to have much a smaller temperature dependence and lower noise floor than Ge photodiodes [3]. Although InGaAs photodiodes are widely used as receivers in optical networks, they have not been extensively evaluated for use in spectroradiometry. Since the detector could be used to assign the spectral radiances of vastly different sources using radiance ratios or signal ratios from one source to another, the linearity of the detectors must be quantified for use in spectroradiometry. In addition, these particular photodiodes have been used as working standards in the key comparison K2.a of the Consultative Committee on Photometry and Radiometry for the intercomparison of spectral power responsivity from 900 to 1600 nm [4]. Since each laboratory participating in the intercomparison could use different optical power levels to assign the spectral responsivity, the determination of the linearity of these InGaAs photodiodes is critical. To our knowledge, there has not been a study of InGaAs photodiode linearity although the linearity of these detectors is an important issue in many applications. The different InGaAs diodes studied and their electrical characterizations are listed in table 1.

The linearity of detectors can be measured with several different techniques. A common technique is to insert a filter into the optical path at different optical power levels. The non-linearity is measured as a change in the filter-in to the filter-out signal ratios. Another well-known method is the beam-flux addition using double apertures. In this study, we use the combination of these two methods with the Beamconjoiner III apparatus developed at the National Institute of Standards and Technology [5].

Although the linearity of photodiodes can also be dependent on the wavelength of the measurements, such wavelength dependences were not investigated during this study. The InGaAs photodiode was illuminated using a broadband source, an FEL lamp, and only a single visible blocking filter was placed in front of the photodiode. All the photodiodes studied had active areas of 5 mm diameter, and the incident flux was made to underfill the diode. Wavelength-dependent non-linearities are possible, especially near the band-gap wavelength of the InGaAs around 1.7 μm.

The linearity of InGaAs photodiodes was determined to an expanded uncertainty of 0.08% ($k = 2$) within the range of photocurrents from 10^{-8} to 10^{-4} A. Below 10^{-8} A, the uncertainty in the linearity measurement is larger due to the increased noise in the photocurrent arising from the feedback resistance of the transimpedance amplifier being greater than the shunt resistance of the photodiode. The shunt resistances

Table 1. The shunt resistances and the shunt capacitances of all the tested photodiodes are shown. The shunt capacitance of the NIST 14 photodiode could not be measured.

Detector	Manufacturer and model	Serial number	Shunt resistance (MΩ)	Shunt capacitance (nF)
NIST 01	Fermionics	123	17.50	1.41
NIST 02	Fermionics	124	12.80	1.43
NIST 03	Fermionics	125	15.40	1.42
NIST 04	GPD GAP5000, D/C 9812	1	1.78	1.33
NIST 05	GPD GAP5000, D/C 9812	2	2	1.1
NIST 06	GPD GAP5000, D/C 9812	3	1.9	1.14
NIST 07	GPD GAP5000, D/C 9812	4	1.8	1.2
NIST 08	EG&G Optoelec. C30723G	6	3.75	0.826
NIST 09	EG&G Optoelec. C30723G	9	5.00	1.50
NIST 10	EG&G Optoelec. C30723G	11	5.71	1.58
NIST 11	EG&G Optoelec. C30723G	13	4.44	1.67
NIST 12	TDC P/N: 35PD5M-TO	2	5	1.8
NIST 13	TDC P/N: 35PD5M-TO	3	2.5	1.87
NIST 14	TDC P/N: 35PD5M-TO	4	0.00125	—
NIST 15	TDC P/N: 35PD5M-TO	5	5	1.85
NIST 16	GPD GAP5000, D/C 9849	11	1.80	1.27
NIST 17	GPD GAP5000, D/C 9849	12	0.58	1.37
NIST 18	GPD GAP5000, D/C 9841	13	1.40	1.44

and the junction capacitances of the photodiodes have also been measured, and the increased noise at the low power levels is correlated with the differences in the respective shunt resistances.

2. Experimental method

The linearity of the InGaAs photodiodes was determined using the Beamconjoiner III apparatus. Our method utilizes a visible-blocking filter (Hoya R72)[1] and reflective neutral density filters to provide 40 different flux values, resulting in 120 different combinations to attenuate the light source, a current-stabilized FEL lamp. The incident light on the InGaAs diodes is broadband infrared with the visible range filtered. The neutral density filters were constructed using metallized quartz substrates for transmission from 0.2 to 2.5 μm. The optical diagram of the Beamconjoiner III is shown in figure 1. The incident flux is introduced into the opening of the light-tight box and is split into two directions by the beamsplitter 1. Each of the filter wheels 1 and 2 has four different reflective neutral density filters with circular openings of 4 cm diameter, and the filter wheel 3 has five filters. Combined with the blocked value for each of the filter wheels, a total of $(5 \times 5 \times 6)$ 150 different combinations can be formed. The filter wheel 3 acts to reduce the total level of the combined flux, and the dynamic range in the optical flux of the highest level to the lowest level is about 500 : 1. The rotation of the filter wheels is controlled using three separate stepper motors, and the rotational positions of the filter wheels are verified with a check of the home position optical switch each time the stepper motor is rotated. The change in the optical flux is performed in the collimated beam before the imaging of the flux onto the detector by the spherical mirror.

[1] Certain commercial equipment, instruments or materials are identified in this paper to foster understanding. Such identification does not imply recommendation or endorsement by the National Institute of Standards and Technology, nor does it imply that the material or equipment are necessarily the best available for the purpose.

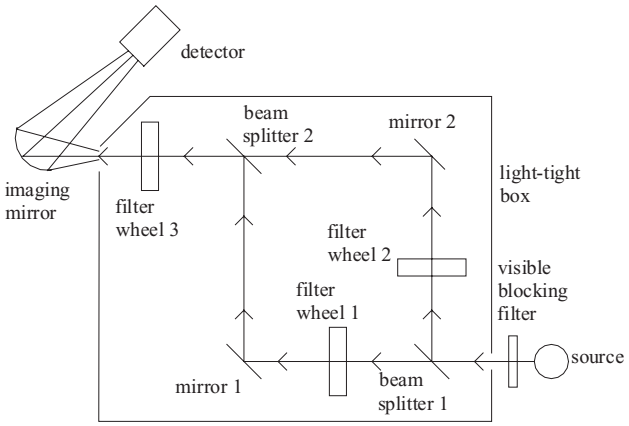

Figure 1. Optical diagram of the Beamconjoiner III apparatus. The source is split into two directions using the beamsplitter 1 and recombined at the detector using beamsplitter 2. The combination of the three filter wheels can produce 120 different signal levels using 40 different flux levels. The optical flux is changed in the collimated beam before imaging onto the detector.

In the measurement protocol, each of the filter wheel positions is assigned a distinct value i, k, j corresponding to the positions of the filter wheel 1, 2, 3, respectively. Each of the 120 different filter combinations is in turn also assigned a distinct number, and the sequence of filter wheel positions for each run is determined using a random number generator prior to each run. Every group of four measurements is followed by a dark measurement, resulting in 30 separate dark measurements for each run. Since each dark signal has a time stamp, any change in the dark signal can be monitored. None of the InGaAs photodiodes discussed in this study showed any evidence of dark signal drift.

Since each run could take up to 1.5 h or longer depending upon the signal averaging needed for optimal signal-to-noise ratios, the source flux has to be temporally stable. The lamp was stabilized by measuring the voltage drop across a calibrated resistor to determine the current, and a closed-loop

current stabilization was used, which adjusted the current every 5 s to the desired value.

Although the power responsivity of the InGaAs photodiodes is temperature sensitive, the photodiodes used in the CCPR K2.a were not operated with temperature stabilization. The temperature was monitored using a thermistor held in contact with the back of the photodiode, and each photodiode was allowed sufficient time to come to temperature equilibrium with the ambient laboratory environment. Temperature changes of the photodiode of few degrees resulted in noisy signal/flux values since the double-beam flux method requires both the source and the detector to be stable during the 120 different measurements.

3. Linearity analysis

Although 150 different signals are possible, only 120 signals are measurements of fluxes from the source. Each signal can be written as a response to the incident flux, or conversely, each flux results in signal as a function of the flux,

$$\begin{aligned}\phi(i,j,k) &= \phi(i,j) + \phi(j,k) \\ &= r_0 + s(i,j,k) + r_2 s^2(i,j,k) + \cdots + r_n s^n(i,j,k) \end{aligned} \quad (1)$$

where $\phi(i,j,k)$ denote the flux, $s(i,j,k)$ is the measured signal at the detector, and $r_0, r_2, \ldots, r_n$ are the coefficients which relate the signal to the flux. The total flux at the detector is a sum of the individual fluxes, $\phi(i,j)$ and $\phi(j,k)$, and flux addition is inherently linear. Since each flux can be an independent flux or sums of independent fluxes, and although 120 signals are measured along with 30 dark signals, only 40 different fluxes exist with 20 fluxes from each of the two paths. Thus equation (1) becomes an over-determined equation with 40 unknown fluxes and one or many unknown coefficients, r_0, $r_2, \ldots, r_n$, but with 120 equations. The unknown fluxes are found by setting up a system of linear equations and performing a least-squares fit of the signals for the 40 unknown fluxes and the coefficients.

Due to the complexity of the matrix inversion and the possibility of errors in the convergence, the analysis program was tested using artificial data sets which simulated the experimental results from the Beamconjoiner. Different constant values were used in the simulations, and second-order correction factors were also simulated. The analysis program was able to correctly converge on all of the coefficients in the artificial data sets.

The determination of linearity is measured using the residuals of the fluxes found using the fit to the measured signal corrected by the appropriate coefficients. Initially, only the constant correction, r_0, is applied and the residuals of the fit,

$$\phi(i,j,k) - [r_0 + s(i,j,k)] \quad (2)$$

are plotted against the signals and examined for indications of the need for higher order corrections. The linearity of the signals is determined from a plot of the ratio of the measured signal to the calculated flux,

$$\frac{s(i,j,k)}{\phi(i,j,k)} \quad (3)$$

and the ratios are fitted using a linear function to determine the uncertainty component of the total signal due to non-linearity. Since flux is inherently linear, and the signals could be nonlinear, any non-linearity of the signal will be evident from the curvature of the ratios.

4. Discussion

A plot of the ratios of the measured signals to the fluxes versus the signals for the NIST 01 photodiode is shown in figure 2. The plot shows signal/flux ratios from three separate runs, each consisting of 120 signal measurements. The measurements were performed using an additional neutral density filter between the filter wheel 3 and the detector to reduce the overall signal such that the wide dynamic range could be spanned from 10^{-9} to 10^{-4} A. The symmetry of the residuals above and below the $y = 0$ axis in figure 2 indicates the goodness of fit, since any non-linearity would be manifest in deviations from a symmetric distribution. From the plot, the detector is determined to be linear from 1×10^{-8} to 1×10^{-4} A in photocurrent with an uncertainty of 0.08% ($k = 2$). The uncertainty is determined from the goodness of a linear fit to the values in the same range.

All the InGaAs photodiodes examined showed linear behaviour with an uncertainty of 0.08% between 5×10^{-8} and 1×10^{-4} A. Some of the photodiodes also exhibited increased noise below 5×10^{-8} A with decreasing photocurrent. A plot of the signal/flux is shown for the detector NIST 18 in figure 3 and shows that the signal to flux ratios below 5×10^{-8} A become noisy as compared to the same measurements of NIST 01. The reasons for the increase in the signal noise will be explored in the noise analysis section of this paper. For example, the Beamconjoiner was used to measure the linearity of silicon photodiodes from 10^{-11} to 10^{-3} A to within 0.054% ($k = 2$), since Si diodes have typical shunt resistances of 1 GΩ [5].

In conjunction with the linearity testing, all the InGaAs photodiodes were also measured for shunt resistance and shunt capacitance. Table 1 shows the measured shunt resistances and the shunt capacitances of the individual InGaAs photodiodes. With the exception of two diodes, NIST 08 and NIST 14, all

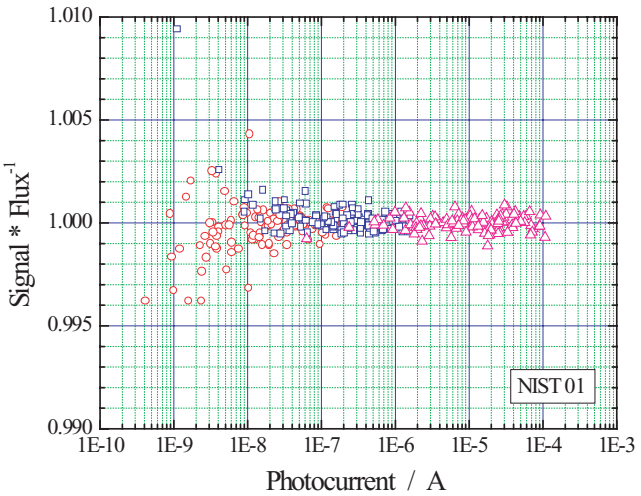

Figure 2. The ratios of the signal divided by the calculated flux plotted versus the signal for the NIST 01 photodiode (17.5 MΩ shunt resistance). A total of three runs are plotted with each run consisting of 120 different signal levels. The ratios can be measured with <0.1% uncertainty for photocurrents below 1×10^{-8} A.

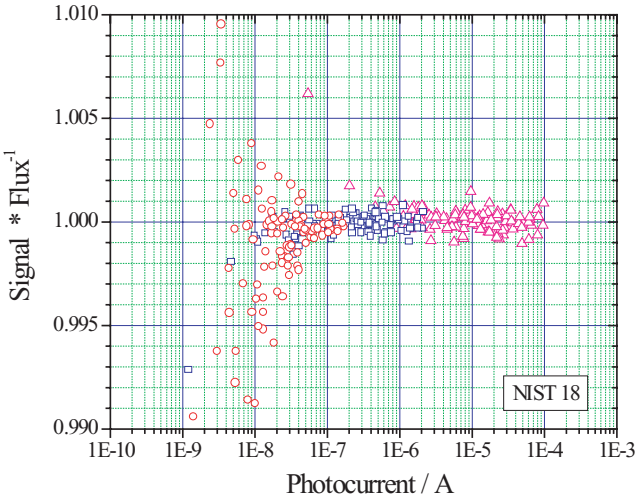

Figure 3. The ratios of the signal divided by the calculated flux plotted versus the signal for the NIST 18 photodiode (1.40 MΩ shunt resistance). The ratios can be measured within the <0.1% uncertainty for photocurrents below 5×10^{-8} A, and the noise increases rapidly at lower photocurrents.

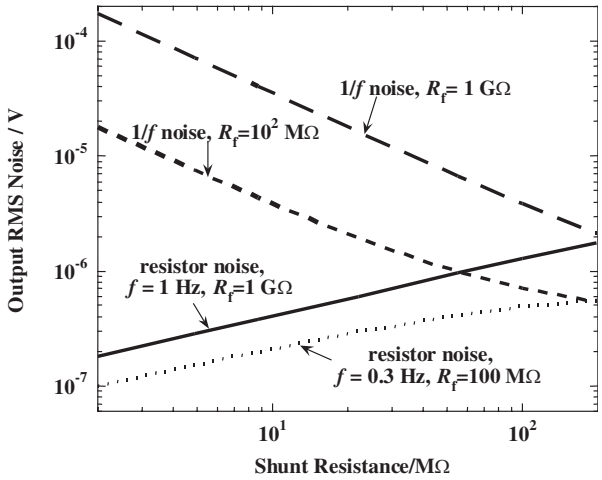

Figure 4. Output root-mean-squared (RMS) noise components of the InGaAs photocurrent meter for the 10^8 and 10^9 V A^{-1} gains versus photodiode shunt resistance.

the diodes had similar shunt capacitances ranging from 1.10 to 1.87 nF. The shunt resistances varied from 0.583 (NIST 17) to 17.5 MΩ (NIST 01).

5. Noise analysis

According to our previous measurements [3], there are two major noise components at the output of an InGaAs photodiode current meter—$1/f$ voltage noise and the resistor noise. The $1/f$ voltage noise arises from the operational amplifier in the current-to-voltage converter. The other major noise component is the resistor noise that is determined by the parallel connection of the detector shunt resistance and the feedback resistance.

Figure 4 shows the two major noise components at the output of the InGaAs photocurrent meter plotted as a function of the shunt resistance. The resistor noise was calculated with two different electrical bandwidths and the output $1/f$ noise was calculated with two different feedback resistors. In the first example; the resistor noise was calculated with 0.3 Hz bandwidth (lowest, dotted curve) and a feedback resistor of $R_f = 100$ MΩ. The output $1/f$ noise, shown with the shorter dashed curve, is independent of the bandwidth selection [6]. The 0.3 Hz bandwidth originates from the 1.7 s integration time (duration of 100 power line cycles) of the DVM connected to the output of the photocurrent meter (current-to-voltage converter). We used 0.35 μV $1/f$ noise in the present calculations. This is a typical value from our earlier measurements on OPA128 and OPA111 operational amplifiers [6]. In the second example, the $1/f$ output noise was calculated with a feedback resistor of 1 GΩ (longer dashed curve on the top). This noise was an order of magnitude larger than that with 100 MΩ. The resistor noise in this case was calculated with a bandwidth of 1 Hz (solid line). The shunt effect of the 1 GΩ feedback resistor for the maximum 200 MΩ shunt resistance was neglected.

Since the resistor noise increases and the voltage amplification decreases with increasing shunt resistance, the output noise could be optimized. In both examples, the two output noise components could be equalized at a shunt resistance of 200 MΩ. The shunt resistance increases when the photodiode is cooled. Our earlier experiments showed that a 2 MΩ shunt resistance at 25°C could be increased to 55 MΩ at a controlled temperature of −30°C [3]. Accordingly, an InGaAs photodiode with 7.3 MΩ shunt resistance at 25°C could produce 200 MΩ shunt resistance at −30°C. A 300 MΩ shunt resistance will equalize the two major output noise components for a 1 GΩ feedback resistor and a bandwidth of 0.3 Hz. To perform the optimization in this third example, an InGaAs photodiode with a shunt resistance of about 11 MΩ at 25°C should be selected. The achievable (equivalent) photocurrent noise at −30°C will be about 1 fA (1 μV/1 GΩ).

In our present linearity measurements, the feedback resistors could be changed from 10^4 to 10^9 Ω. At the 100 MΩ and 1 GΩ gain selections, the resistor noise was dominated by the photodiode shunt resistance. The shunt resistance at room temperature was smaller than 20 MΩ for all measured photodiodes. At the low gain selections, where the feedback resistor was smaller than the shunt resistance, the resultant resistance was dominated by the feedback resistor. At these gain selections, the voltage amplification for the $1/f$ input voltage noise was close to unity. Accordingly, resistor noise and output $1/f$ noise were similar for the shunt resistance interval (about one decade) shown in table 1. For detectors with small shunt resistance, the voltage amplification at high feedback resistor selections can be very large, resulting in a dominating $1/f$ noise component in the output signal. This is why the noise floor of the NIST 18 photodiode was an order of magnitude higher than that of the NIST 01.

6. Conclusion

The linearity and signal dynamic range of 18 InGaAs photodiodes have been studied. The major noise components of the InGaAs photocurrent meters were analysed versus shunt resistance, signal gain and bandwidth. A limit sensitivity of 1 fA can be achieved at 10^9 V A^{-1} gain if the amplified $1/f$ noise and the resistor noise are equalized at the output of the

current meter. For the tested room temperature photodiodes, linearity could be measured from 10^{-8} to 10^{-4} A with an expanded uncertainty of 0.08% ($k = 2$). When the shunt resistance was increased by cooling one of the photodiodes, the linearity measurement range could be extended a decade due to the increase of the shunt resistance.

References

[1] Gutschwager B and Fischer J 1999 An InGaAs radiation thermometer with an accurate reference function as transfer standard *Proc. TEMPMEKO '99 (Delft, Netherlands)* ed J F Dubbledam and M J deGroot

[2] Yoon H W, Proctor J E and Gibson C E 2003 FASCAL 2: A new NIST facility for the spectral irradiance calibrations of sources *Metrologia* **40**

[3] Eppeldauer G 1997 Electronic characteristics of Ge and InGaAs radiometers *Proc. SPIE* **3061** 833–8

[4] Larason T C, Brown S W and Lykke K R 2002 InGaAs photodiodes used in a CCPR near-infrared key comparison *Metrologia Proc. NEWRAD02 (Gaithersburg, MD)*

[5] Thompson A and Chen H M 1994 Beamcon III, a linearity measurement instrument for optical detectors *J. Res. Natl. Inst. Stand. Technol.* **99** 751–5

[6] Eppeldauer G and Hardis J E 1991 Fourteen-decade photocurrent measurements with large-area silicon photodiodes at room temperature *Appl. Opt.* **30** 3091–9